Spectrochimica Acta Part A: Molecular and Biomolecular Spectroscopy 261 (2021) 120034

Contents lists available at ScienceDirect

Spectrochimica Acta Part A: Molecular and Biomolecular Spectroscopy

journal homepage: www.elsevier.com/locate/saa

Fabrication and measurement of fiber optic localized surface plasmon resonance sensor based on gold nanoparticle dimer

Hyeong-Min Kim, Jae-Hyoung Park *, Seung-Ki Lee *

Department of Electronics and Electrical Engineering, Dankook University, Yongin 16890, South Korea

HIGHLIGHTS

- We fabricate the dimers of gold nanoparticles on the optical fiber with simple method.
- The longitudinal band displays approximately 9.1 times higher sensitivity.
- The dimer-based fiber optic LSPR sensor proves an improved LOD of about 2.6 times.
- Selectivity was evaluated and the validation was made on real samples.

GRAPHICAL ABSTRACT

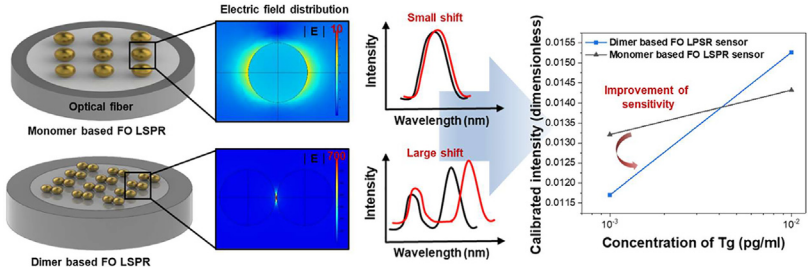

ARTICLE INFO

Article history:
Received 29 March 2021
Received in revised form 12 May 2021
Accepted 27 May 2021
Available online 29 May 2021

Keywords:
Biosensor
Dimer
Localized surface plasmon resonance
Miniaturization
Optical fiber

ABSTRACT

Fiber optic localized surface plasmon resonance (FO LSPR) sensors capable of portable, real-time, and remote sensing are emerging with the progress of lab-on-fiber technology. However, the small area of the substrate by the optical fiber often restricts the sensitivity of the FO LSPR sensors. To improve the performance of the FO LSPR sensors, it is necessary to enhance the interactions between incident light and plasmonic nanostructures within a defined region. Dimer in which two nanoparticles are arranged with nanometer spacing can effectively increase the light-nanostructure interactions. It is well known that the nanogap made in the assembled nanoparticles significantly enhances the intensity of the electromagnetic field in the confined area by the hot spot effect. We fabricate the dimers of gold nanoparticles on the optical fiber with benzenethiol using a method that reduces the repulsive force between the nanoparticles. In the dimers, the strong plasmonic interaction between the two nanoparticles produces a longitudinal plasmon coupling band, which is compared to the transverse plasmon band by the monomer-based FO LSPR sensor with a similar density of gold nanoparticles. In the proposed sensor, the longitudinal band displays approximately 9.1 times improved sensitivity. When two types of sensors are applied to the biosensor application, the dimer-based FO LSPR sensor also proves an improved limit of detection of about 2.6 times. This method is expected to become a milestone in the field of measurement for small molecules and low concentration through the advancement of the yield and density of dimers.

1. Introduction

The fiber optic sensor, which observes the intensity [1,2], phase [3], or frequency [4] of reflected or transmitted light has been widely applied as a tool for bio-applications with properties such as simplification of the optical system, small loss in signal, chemical resistance, and biocompatibility [5–7]. Recently, the fiber optic localized surface plasmon resonance (FO LSPR) sensor is attracting attention as a biosensor with several distinct advantages that require non-labeling, enable real-time monitoring, and allow a small volume for analysis [8–10]. LSPR is the collective resonance of conduction electrons by excitation in noble metal nanoparticles

* Corresponding authors.
E-mail addresses: parkjae@dankook.ac.kr (J.-H. Park), skilee@dankook.ac.kr (S.-K. Lee).

https://doi.org/10.1016/j.saa.2021.120034
1386-1425/

having a size smaller than the wavelength of light [11]. The resonance band in the scattering and absorption by the incident light are shifted according to the quantity by immunoreaction with the target molecules when the receptors are fixed to the noble metal nanoparticles, which are coated on the optical fiber. Therefore, the antigen concentrations can be determined by measuring the band shifts [12,13]. The shift of the resonance band involves variations in wavelength and intensity, and it has been reported that the observation of the intensity difference is more advantageous in detecting the small refractive index change due to biomarker adsorption [14].

Despite the various advantages of the FO LSPR sensor, the sensitivity is often limited because of the narrow sensing area by the small diameter of the optical fiber [15,16]. To improve the sensitivity of the FO LSPR sensor, methods that modify the shape of the optical fiber are tried. The middle of the optical fiber is stretched, the tip-end is transformed into a cone shape, or the polished area of the cladding is expanded [17–19]. However, the methods by structure modification break the precise matching for total reflection between the core and cladding, which can adversely affect the transmission and stability of the optical signal. As another solution for enhancing the sensitivity, plasmon coupling due to the interferences between metal nanoparticles has lately been illuminated, which can generate a longitudinal LSPR peak in the relatively long wavelength region [20–22]. Generally, the coupling between surface plasmons occurs in the dimer with nanometer-scale distance, which is the most representative structure for the induction of longitudinal band [23]. In the nanogap between the particles, a phenomenon in which the electromagnetic field is amplified is also observed, which is called the hot spot effect [24]. It is typically known that the peak in the longitudinal mode caused by the plasmon coupling is highly sensitive to the change in the refractive index around the nanoparticles [25–27].

In this paper, we fabricate the dimers on optical fiber with an acceptable yield by using a simple method [28], that reduces the repulsive force between the particles during the first immobilization of gold nanoparticles (AuNPs) and the second fixation of AuNPs. The condition is modified by analyzing the sensitivity of the sensor according to the second coating time of AuNPs. After determining the primary and secondary attachment times of the nanoparticles, a monomer-based FO LSPR sensor having the same total immobilization time of the AuNPs was additionally fabricated without the reduction treatment of the repulsive force. The sensitivities in the refractive index are measured and compared at the dimer-based FO LSPR sensor and the monomer-based FO LSPR sensor, respectively. Two types of sensors are also applied to survey the antibody-antigen interactions, where the derived limit of detections (LODs) are evaluated. By introducing the dimers of AuNP on an optical fiber, the fabricated sensor is expected to be spent to the lab-on-fiber based the biosensing field that requires highly sensitive measurements.

2. Materials and methods

2.1. Materials

Sodium citrate dihydrate (>99.0%), ethyl alcohol anhydrous (>99.5%), and glycerol (≥99.0%) were purchased in Daejung Chemical, South Korea. Gold (III) chloride trihydrate (≥99.9%), poly(4-vinyl pyridine) (P4VP, the average molecular weight of ~ 160,000), benzenethiol (≥98%), and bovine serum albumin (BSA, ≥98%) were obtained from Sigma Aldrich, USA. Borate buffer (pH 8.5, 50 Mm) was bought in Bioworld, USA. Antibody and Antigen of thyroglobulin (Tg) were gained in commercial kit of Fujirebio, Japan. Antigen of alpha-fetoprotein (APF) was acquired in Shin Jin Medics, South Korea. Polydimethylsiloxane (PDMS) base (Sylgard 184A) and PDMS curing agent (Sylgard 184B) were supplied in Dow Corning, USA. Slide glass (size: 26 mm × 76 mm, thickness: 1.0 ± 0.05 mm) was produced in Duran, Germany. The optical fiber (FG105LCA, core diameter: 105 μm) was purchased in Thorlabs, USA. Deionized (DI) water (resistivity: 18.2 MΩ·cm) was produced by a water purification system (Aqua MAX^{TM}-ultra, Youngin Chromass, South Korea).

2.2. Fabrication of dimers of AuNP on optical fiber

The fabrication process of AuNP dimers on optical fiber consists of three steps: the first immobilization of AuNP layer, benzenethiol coating, and the second fixation of AuNPs. The schematic diagram of the manufacturing technique is illustrated in Fig. S1.

First, the cross-section of the fiber from which the jacket of the end has been removed reacted with piranha solution (1:3 volumetric ratio of hydrogen peroxide and sulfuric acid) for 20 min. This action is to eliminate contaminants on the end-face of the optical fiber and functionalize the surface as hydrophilicity. Then, the optical fiber was immersed in a 0.3% P4VP alcoholic solution. At this time, pyridine molecules are densely coated on the fiber end-facet [29]. After 30 min, the surface was washed sequentially with ethanol and DI water. Finally, the AuNPs were attached as the optical fiber was stored in a gold colloid for 60 min. The colloidal solution was synthesized by mixing a 0.01% chloroauric acid in an aqueous medium heated to 100℃ and a 1% aqueous solution of sodium citrate at a volume ratio of 100:1. The reaction was terminated within 20 min with vigorous stirring and cooled to room temperature. The solution color changes from yellow to wine red. This condition guarantees a particle size around 55 nm. It has been confirmed that this size ensures measurement reproducibility with robustness for fabrication environment in a constructed set-up based on the previous study [30]. The prepared gold colloid was centrifuged at 5000 rpm for 15 min (mySPIN12, Thermo Fisher Scientific, USA), which was redispersed in DI water. This process was repeated twice and it was stored at 4℃ until use. When the buffer solution is not replaced, other ions generated during the preparation of the colloidal solution can cause aggregation and migration of AuNPs on the surface of the optical fiber [31], which especially affects the second immobilization process of AuNPs. The lone pair of nitrogen atoms in the pyridine ring ionically adsorbs the AuNPs onto the fiber end-face [32]. The nanoparticles produced by the citrate reduction method have negative surface charges.

When AuNPs are again coated on the surface having previously fixed nanoparticles without any treatment, most of the AuNPs exist as monomers due to the repulsive force between the particles, since the nanoparticles are capped by negative charges. In order to reduce the repulsive force between the AuNPs, a low concentration of benzenethiol was coated on the first attached particles. Before the second fixation of the AuNPs, the optical fiber with a once immobilized AuNP layer was kept in a 100 nM benzenethiol alcoholic solution for 24 h. After that, the fiber optic end-facet was flushed with ethanol and DI water, respectively.

To fabricate the dimer-based FO LSPR sensor, the optical fiber was once again dipped in a gold colloid for 45 min, 60 min, 90 min, 120 min, and 150 min, respectively. Some of the secondly absorbed nanoparticles formed dimers with initially attached AuNPs because of the weakened repulsive force on the particle surface by benzenethiol molecules.

2.3. Set-up for measurement

Fig. 1 demonstrates the set-up for optical measurement containing the microfluidic system. White light (LS-1, Ocean Optics, USA) was used to excite the AuNPs on the surface of the optical

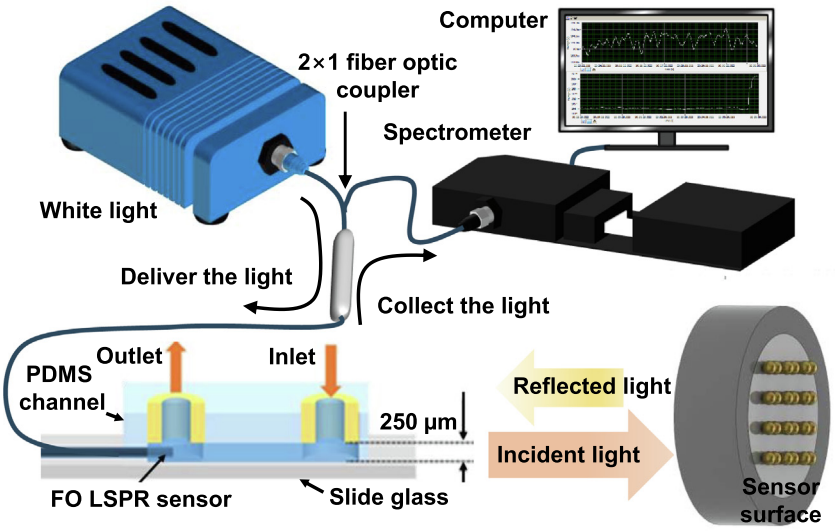

Fig. 1. Optical measurement system. Light is transmitted to the sensor surface through a fiber optic coupler and the scattered light is collected in a spectrometer.

fiber. To observe the spectra of the monomer and dimer of AuNP, a spectrometer (SM200, Spectral Products, USA) was operated, and the spectra were expressed through the SM32Pro software of a computer. A 2 × 1 fiber optic coupler was used to connect the light source, detector, and FO LSPR sensor. The 2 × 1 fiber optic coupler was made to order in Thorlabs. One end in the two-port ends is FC/PC connector, which is joined to the white light. FC and PC are acronyms for fiber channel and physical contact, respectively. The other side is equipped with a SubMiniature version A patch cable and is linked to the spectrometer. To splice the fabricated FO LSPR sensor, one-port end does not have a cable. The signal which is absorbed in the fiber optic sensor surface is carried to the source and detector in a 50:50 ratio. The optical fiber type used in fabrications of sensor and coupler is a standard glass-clad silica multimode fiber and has a 0.22 numerical aperture. The spectrometer involves a wavelength range from 300 nm to 900 nm. Its spectral resolution is 1.5 at a wavelength of 546 nm and wavelength resolution is 0.5 nm. Measurements were carried out in the PDMS microfluidic channel to prevent degradations of measurement reproducibility due to evaporation and contamination of the reagents concerning exposure to the external environments of the FO LSPR sensor [33]. The fluidic chip was fabricated by plasma bonding (time: 40 s, pressure: 0.1 Torr, power: 60 W, CUTE, Femto Science, South Korea) of the slide glass and PDMS channel, which is widely known as a transparent and biocompatible material [34]. The height and width of the path inside the channel are 250 μm equal to the fiber optic thickness including the jacket. The inlet and outlet were opened by a biopsy punch (15110–15, Ted Pella, USA) with an inner diameter of 1.5 mm.

2.4. Protocol for measuring the response by antibody-antigen interaction

The protocol for quantitatively measuring the bound antigen to the FO LSPR sensor is divided into 4 steps. First, the intensity in DI water was at least recorded for 5 min as a baseline, which is later utilized to calibrate the signal difference by antigen binding [35]. In this study, several sensors were fabricated in one batch using the solution process, and an individual sensor is consumed for separate measurement [35]. Although the sensors are manufactured in the same batch, the distribution of AuNPs on the optical fiber cannot be identical, which appears as the difference in the baseline. The magnitude of the signal measured in DI water can partially reflect the distribution and density of nanoparticles on the fiber optic surface because DI water does not contain any ions. If the baseline intensity in a specific sensor is larger than that of other samples, this indicates an increase in the number of AuNPs and dimers on the end-face of the optical fiber, which means an enhancement in sensing area and efficiency. Here, measurement reproducibility can be reduced when the same concentration is repeatedly detected by an individual sensor, because the amount of signal difference by antigen binding is increased only in an arbitrary sensor by the improved sensing area and efficiency. We calibrate the influence of non-reproducibility, which occurs in the fabrication process of the FO LSPR sensor by dividing the net change of the intensity due to the antibody-antigen reaction using the baseline. Then, 20 μg/ml antibody solution in borate buffer was injected into the sensor surface for 15 min. The flow rate was 10 μl/min. Antibodies were electrostatically adsorbed on the AuNP surface because the Tg antibody contains positive charges with amine groups in borate buffer [36]. Excess antibodies were washed with DI water. Next, BSA that is an efficient blocking agent was fed for 15 min to suppress nonspecific binding between the sensor surface and the antigen [37]. The concentration of BSA solution was 1% and unbound BSAs were flushed by DI water. Finally, the antigen solution was only supplied for 5 min to induce a specific interaction of the antibody-antigen. The short reaction time is an advantage due to the narrow area of the optical fiber. Unconjugated antigens were rinsed with DI water. The difference in the intensity measured in DI water before and after the immune interaction is defined as the output by the amount of antigen binding. The spectra and signal trend recorded in real-time during a series of reactions for immunoassay is attached to Fig. S2.

3. Results and discussion

3.1. Modification in the second fixation time of AuNPs

The fabrication condition of the dimer-based FO LSPR sensor was modified by varying the second fixation time of AuNPs, after the reduction treatment of the repulsion with benzenethiol was performed on pre-fixed AuNPs in optical fiber. The first immobilization time of AuNPs and the benzenethiol coating state were maintained, and the condition related to the second fixation of

nanoparticles was only changed. In Fig. 2, no meaningful signals were observed in the 45 min and 60 min samples of the secondary fixation time due to the insufficient density of dimers, where longitudinal bands were ambiguous to be recorded. In samples of 90 min, 120 min, and 150 min, peaks were distinguished not only in the relatively short wavelength region by transverse mode but also in the long wavelength area by the longitudinal mode of the dimer. Sensitivities (slopes), which are defined as the rate of change in the output intensity versus the variation in the refractive index, were compared on the basis of the peaks in the longitudinal band in three conditions of dimer-based FO LSPR sensors [38]. The range of measured refractive indices was from 1.34 to 1.38 with an interval of 0.01, where the refractive index solutions were prepared by adding glycerol to DI water [39]. To compare the relative change in refractive index responses under three conditions, the intensities measured in each sensor were normalized due to the recorded signal in the 1.34 refractive index [40]. As a result, the dimerization condition with a secondary attachment time of 90 min displayed a higher sensitivity than other samples. The second fixation time of AuNPs was set as 90 min though the fabrication yield of the dimer slightly increased with a longer fixation time. The best performance in 90 min condition was due to the bigger influence of the background by the increase in the number of monomers and multimers than the improvement in dimer yield by prolonged fixation time. In the second fixation process of AuNPs, dimers are formed with existing monomers, but newly immobilized monomers are also generated. When the immobilization time increases, correspondingly multimers except for the dimer can be as well produced. The dense AuNPs by the lengthened immobilization time in the two-dimensional plane of the same region causes an increase in the magnitude of the LSPR intensity, but this does not guarantee an improvement in sensitivity without coupling or amplification of the electromagnetic field [41].

3.2. Fabrication result of AuNP dimers on optical fiber

The field-emission scanning electron microscope (FE-SEM, S-5200, Hitachi, Japan) image after the first immobilization of the AuNP layer is shown in Fig. 3(a). The average size of AuNPs on optical fiber was analyzed as 59.2 ± 9.9 nm by FE-SEM photograph. The nanoparticles were evenly distributed on the fiber optic cross-section without large clustering. When the AuNPs were re-immobilized without the reduction of repulsive force by benzenethiol, monomers will be mainly observed. This phenomenon is confirmed in Fig. 3(b), where AuNPs were firstly fixed for 60 min on the fiber optic surface and secondly immobilized for 90 min without benzenethiol treatment. This was later compared to the dimer-based FO LSPR sensor as the monomer-based fiber optic sensor having a similar density of AuNPs. Pictures of the dimers obtained by the simple treatment for a repulsive force reduction between the first and second immobilized nanoparticles are indicated in Fig. 3(c) and (d). The ratio of dimer at the fiber optic surface was approximately 46.3% based on the FE-SEM images. A histogram of the distribution of the AuNP shape is illustrated in Fig. S3. A higher yield of dimers on optical fiber can be achieved by modifying the concentration of the colloidal solution, the reagent for decreasing the repulsive force, and the immobilization time of the particles.

3.3. Refractive index measurement and comparison of the results by monomer and dimer-based FO LSPR sensors

For characteristic analysis as a refractometer, various refractive indices were measured using a monomer and dimer-based FO LSPR sensor having the same immobilization time of AuNPs. In the monomer-based FO LSPR sensor (Fig. 4(a)), the resonance peak was observed at about 585 nm, which is within the commonly known peak wavelength range due to LSPR in gold nanospheres [42]. In the dimer-based FO LSPR sensor of Fig. 4(b), the longitudinal band (726.5 nm) was found in the long wavelength region as well as the transverse band (557.5 nm) in the short wavelength area. The LSPR intensities linearly changed with the increase of the refractive indices in both types of sensors. The sensitivities were illustrated on the basis of the resonance peaks which are perceived at the spectra by each sensor (Fig. 4(c)). To compare the relative change in the three resonance bands (transverse mode by monomer-based structure, transverse mode by dimer-based structure, longitudinal mode by dimer-based structure), the measured intensities were divided by the intensity of 1.34 refractive index in each sensor. Based on the transverse mode, the dimer-based structure had a 2.1 times higher sensitivity than the monomer-based sensor. Sensitivity enhanced up to 9.1 times in the longitudinal mode of the dimer-based FO LSPR sensor. This was also supported by a simulation grounded by electromagnetic wave, frequency domain model (Fig. S4). With reference to these results, the monomer and dimer-based FO LSPR sensors were applied to the measurement of the antibody-antigen interaction, respectively.

3.4. Immunoassay by monomer and dimer of AuNP

Each FO LSPR sensor based on the monomer and dimer of AuNPs was applied to detect Tg known as a thyroid cancer biomar-

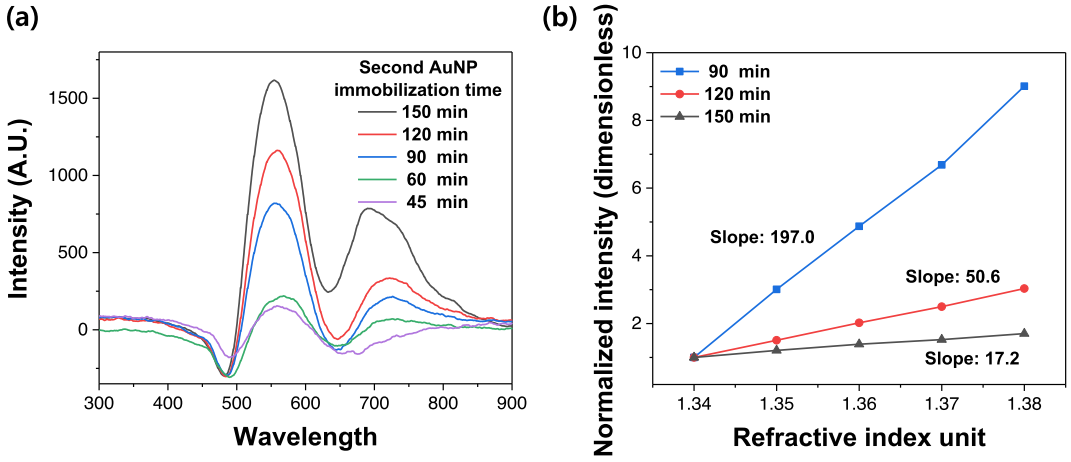

Fig. 2. Spectra and sensitivities when the secondary fixation time of AuNPs is different: (a) measured spectra and (b) refractive index sensitivities based on the longitudinal band of each sensor.

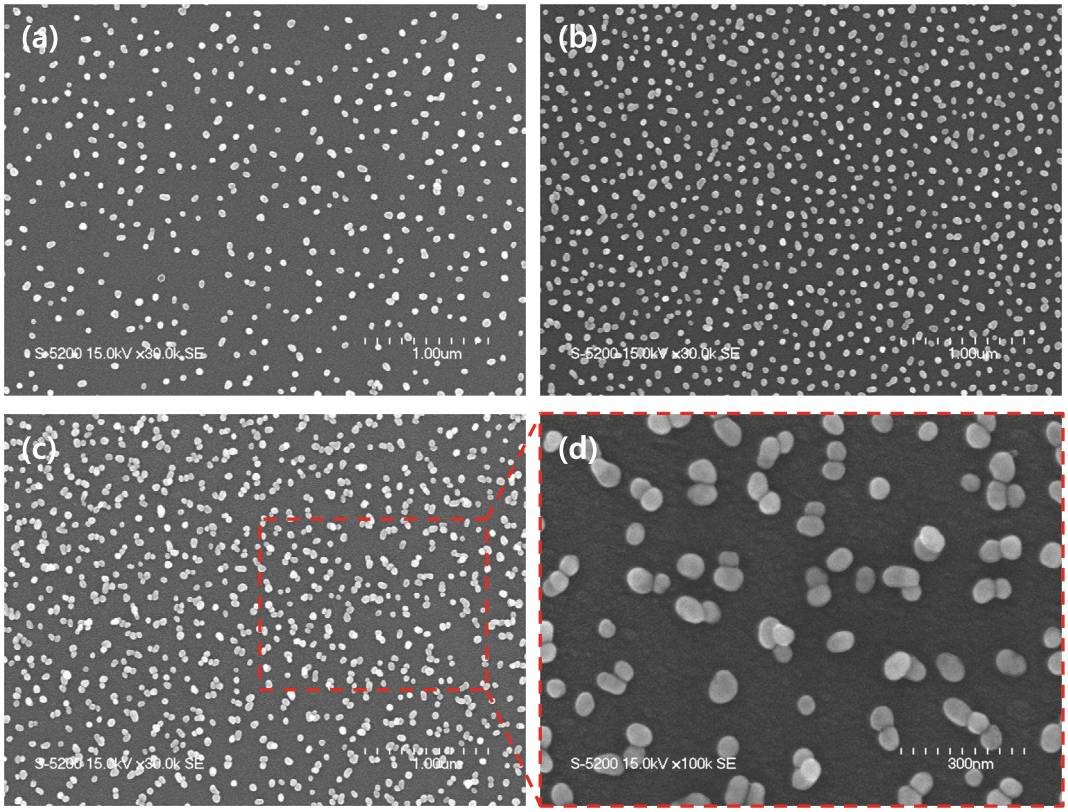

Fig. 3. The FE-SEM images of the cross-section of the optical fiber: (a) after the first immobilization of AuNP layer, after the second fixation of AuNPs (b) without benzenethiol treatment, and (c) with benzenethiol coating and (d) its enlarged picture.

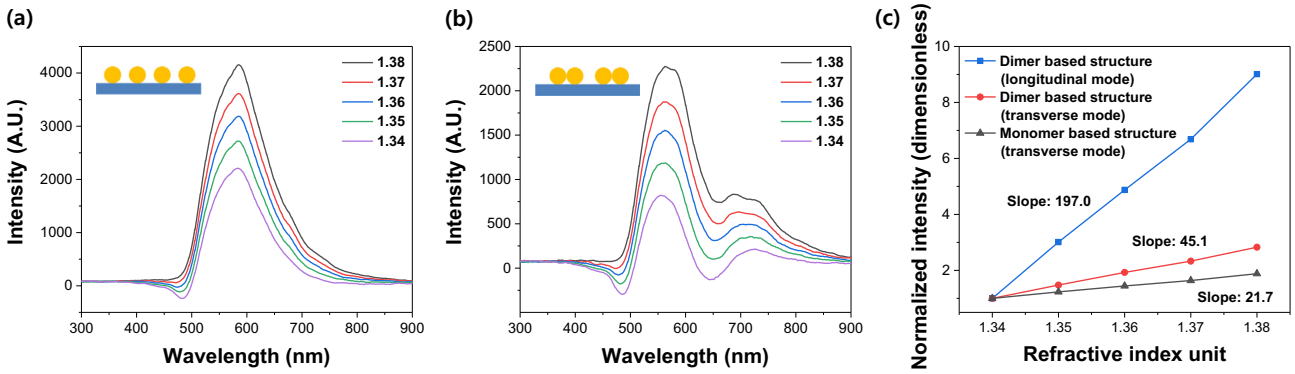

Fig. 4. Results of refractive index measurement by monomer and dimer-based FO LSPR sensors: the measured spectra from the (a) monomer and (b) dimer of AuNPs, (c) sensitivities obtained in resonance bands of each sensor.

ker [43]. For comparison of the limit of detection, only the low range of thyroglobulin levels was measured. The LODs were calculated by linearly fitting the graphs in Fig. 5(a) based on the slope and three times the standard deviation [44]. In the monomer-based FO LSPR sensor, the LOD of 0.13 pg/ml was obtained. By detecting the change of intensity in the longitudinal mode of the dimer structure as a function of the concentration of the protein, we evaluated the LOD as 0.050 pg/ml. As a result, the 2.6-fold improved LOD was acquired due to the strengthened electromagnetic field in the dimer's longitudinal plasmon coupling band. The large slope in the dimer-based FO LSPR sensor of Fig. 5(b) corroborates the enhanced LOD. The performance of the proposed sensor has a chance to be further enhanced by increasing the fabrication yield of the dimer on fiber optic end-facet. It is expected that the FO LSPR sensor based on the dimer structure of nanoparticles with narrow spacing will be worthily expended for applications that require high sensitivity.

For evaluation of the analytical performance in the designed method, non-specific binding was induced between the dimer-based biosensor with Tg antibody and other antigen. After adsorbing Tg antibodies onto the dimer surface, we detected AFP which is a biomarker of liver cancer (Fig. 6). The experiments were proceeded in the same concentration range at which Tg was measured. It is known that the level of AFP in the body also changes depending on the effects of thyroid disease [45]. Therefore, Tg sensors need the selectivity for AFP. The developed sensor did not exhibit a particular tendency according to the concentration of different antigens, which ensures the specificity of the dimer-based

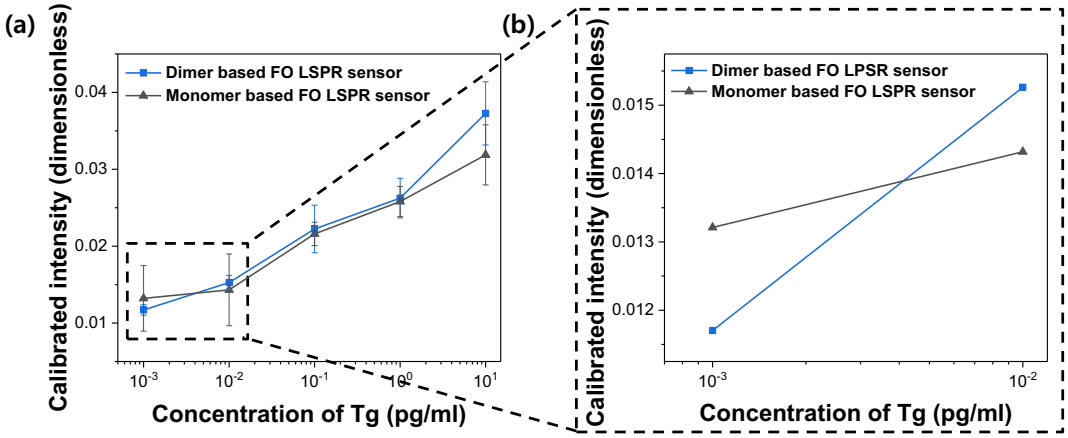

Fig. 5. Net changes of intensity by antigen binding: (a) The various concentrations of Tg were detected by monomer and dimer-based FO LSPR sensors., (b) The averages of measured values in 1 fg/ml and 10 fg/ml of Tg were shown in enlarged view.

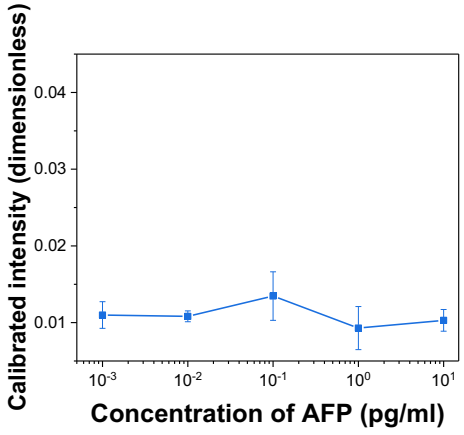

Fig. 6. Non-specific binding of the fabricated dimer-based FO LSPR sensor to another antigen.

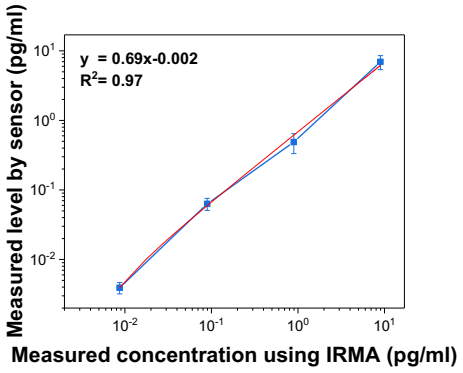

Fig. 7. Tg measurement results in real samples. The results were compared with the values derived by commercial method.

FO LSPR sensor and sensing protocol. Based on these results, the proposed sensor can be a feasible attempt to analyze Tg in the actual application.

3.5. Analysis of real samples

The proposed method was validated by measurement of the real sample and comparison with a standard method. Serum samples of four patients with Tg concentrations from 8 ng/ml to 9 ng/ml were diluted to four levels ranging from 0.001 pg/ml to 10 pg/ml. Each point was detected three times. The FO LSPR sensor output measured in the real samples was converted to concentration using the graph of Fig. 5(a) and linear equation. In Fig. 7. the obtained concentrations by dimer-based FO LSPR sensors were compared with the those of commercially available immunoradiometric assay (IRMA) kit (RIAKEY Thyroglobulin IRMA Tube, Shin Jin Medics, South Korea). A high correlation was found with a coefficient of determination (R^2) of 0.97 between the concentrations detected by the two methods. When the graph of Fig. 7 is fitted with a linear equation, the slope was 0.69, which means that the proposed sensor slightly underestimates the concentrations of the sample. This is because of dilution in the serum samples and can be improved by introduction of appropriate compensation factors [46]. The coefficient of variation (CV) was calculated to verify reproducibility. The average of the CVs in the four points was 20.0%. This is a satisfactory reliability for analyzing real samples in the field of biosensing research [47].

4. Conclusion

In this study, the dimer structure by AuNPs was fabricated on the optical fiber to improve the sensitivity of the optical fiber based LSPR sensor, because the sensitivity of the fiber optic sensor was often limited by the small dimension. It is known that the longitudinal band in the spectrum by the dimer structure, which is observed at a relatively long wavelength, is highly sensitive to the changes in the surrounding environment. After the first immobilization of the AuNPs on the optical fiber, benzenethiol treatment was performed to reduce the repulsive force with the nanoparticles to be secondly fixed. Then, dimers were fabricated through the combination with the pre-fixed nanoparticles when the second attachment of AuNPs was performed. The proposed sensor demonstrated enhanced sensitivity when compared to the monomer-based FO LSPR sensor with the same immobilization time of AuNPs. Accordingly, a lower LOD was acquired in the dimer-based FO LSPR sensor when the immune interaction was detected by both sensors, respectively. This study paves the way for the fabrication of dimers on the optical fiber for high sensitivity and should lead to further studies to optimize fabrication and condition for improved yield and density of the dimer.

CRediT authorship contribution statement

Hyeong-Min Kim: Validation, Investigation, Data curation, Writing - original draft. **Jae-Hyoung Park:** Conceptualization, Methodology, Writing - review & editing, Supervision, Resources, Project administration. **Seung-Ki Lee:** Conceptualization, Methodology, Writing - review & editing, Supervision, Resources, Project administration.

Declaration of Competing Interest

The authors declare that they have no known competing financial interests or personal relationships that could have appeared to influence the work reported in this paper.

Acknowledgements

This work was supported by the National Research Foundation of Korea (NRF) grant funded by the Korea government (MSIT) (No. NRF-2018R1A2B6001361 and NRF-2019R1A2C1083969). The authors appreciate Prof. Jung-Mu Kim at the Division of Electronics and Information Engineering, Chonbuk National University for the computational simulation support.

Appendix A. Supplementary data

Supplementary data to this article can be found online at https://doi.org/10.1016/j.saa.2021.120034.

References

[1] X. Li, Y. Shao, Y. Yu, Y. Zhang, S. Wei, A highly sensitive fiber-optic Fabry-Perot interferometer based on internal reflection mirrors for refractive index measurement, Sensors 16 (2016) 794.
[2] J.S. Velázquez-González, D. Monzón-Hernández, D. Moreno-Hernández, F. Martínez-Piñón, I. Hernández-Romano, Simultaneous measurement of refractive index and temperature using a SPR-based fiber optic sensor, Sens. Actuators B Chem. 242 (2017) 912–920.
[3] S. Wang, X. Fan, Q. Liu, Z. He, Distributed fiber-optic vibration sensing based on phase extraction from time-gated digital OFDR, Opt. Express 23 (2015) 33301–33309.
[4] Z. Chen, G. Hefferman, T. Wei, Terahertz-range weak reflection fiber optic structures for sensing applications, IEEE J. Sel. Top. Quantum Electron. 23 (2016) 246–251.
[5] J.M. López-Higuera, L.R. Cobo, A.Q. Incera, A. Cobo, Fiber optic sensors in structural health monitoring, J. Light. Technol. 29 (2011) 587–608.
[6] B.H., Lee, Y.H. Kim, K.S. Park, J.B. Eom, M.J. Kim, B.S. Rho, H.Y. Choi, Interferometric fiber optic sensors, Sensors 12 (2012) 2467-2486.
[7] D.R. Raj, S. Prasanth, T.V. Vineeshkumar, C. Sudarsanakumar, Surface plasmon resonance based fiber optic sensor for mercury detection using gold nanoparticles PVA hybrid, Opt. Commun. 367 (2016) 102–107.
[8] A.K. Sharma, A.K. Pandey, B. Kaur, A review of advancements (2007–2017) in plasmonics-based optical fiber sensors, Opt. Fiber Technol. 43 (2018) 20–34.
[9] H.I. Muri, A. Bano, D.R. Hjelme, A single-point, multiparameter, fiber optic sensor based on a combination of interferometry and LSPR, J. Light. Technol. 36 (2018) 1159–1167.
[10] S. Kaye, Z. Zeng, M. Sanders, K. Chittur, P.M. Koelle, R. Lindquist, U. Manne, Y. Lin, J. Wei, Label-free detection of DNA hybridization with a compact LSPR-based fiber-optic sensor, Analyst 142 (2017) 1974–1981.
[11] C. Boerigter, R. Campana, M. Morabito, S. Linic, Evidence and implications of direct charge excitation as the dominant mechanism in plasmon-mediated photocatalysis, Nat. Commun. 7 (2016) 1–9.
[12] S.M. Yoo, D.K. Kim, S.Y. Lee, Aptamer-functionalized localized surface plasmon resonance sensor for the multiplexed detection of different bacterial species, Talanta 132 (2015) 112–117.
[13] M. Focsan, A.M. Craciun, M. Potara, C. Leordean, A. Vulpoi, D. Maniu, S. Astilean, Flexible and tunable 3D gold nanocups platform as plasmonic biosensor for specific dual LSPR-SERS immuno-detection, Sci. Rep. 7 (2017) 1–11.
[14] J. Yan, P. Liu, Z. Lin, G. Yang, New type high-index dielectric nanosensors based on the scattering intensity shift, Nanoscale 8 (2016) 5996–6007.
[15] Y.C. Chang, H.C. Chung, S.C. Lu, T.F. Guo, A large-scale sub-100 nm Au nanodisk array fabricated using nanospherical-lens lithography: a low-cost localized surface plasmon resonance sensor, Nanotechnol. 24 (2013) 095302.
[16] I. Antohe, D. Spasic, F. Delport, J. Li, J. Lammertyn, Nanoscale patterning of gold-coated optical fibers for improved plasmonic sensing, Nanotechnol. 28 (2017) 215301.
[17] B.D. Gupta, C.D. Singh, A. Sharma, Fiber optic evanescent field absorption sensor: effect of launching condition and the geometry of the sensing region, Opt. Eng. 33 (1994) 1864–1869.
[18] H.H. Jeong, Y.J. Son, S.K. Kang, H.J. Kim, H.J. Roh, N. Erdene, J.H. Park, D.H. Jeong, H.Y. Lee, S.K. Lee, Fiber-optic refractive index sensor based on the cone-based round structure, IEEE Sens. J. 13 (2012) 351–358.
[19] J. Chen, S. Shi, R. Su, W. Qi, R. Huang, M. Wang, L. Wang, Z. He, Optimization and application of reflective LSPR optical fiber biosensors based on silver nanoparticles, Sensors 15 (2015) 12205–12217.
[20] X. Li, S. Guo, C. Kan, J. Zhu, T. Tong, S. Ke, W.C.H. Choy, B. Wei, Au Multimer@MoS_2 hybrid structures for efficient photocatalytical hydrogen production via strongly plasmonic coupling effect, Nano Energy 30 (2016) 549–558.
[21] T. Lahtinen, E. Hulkko, K. Sokołowska, T.R. Tero, V. Saarnio, J. Lindgren, M. Pettersson, H. Häkkinen, L. Lehtovaara, Covalently linked multimers of gold nanoclusters Au_{102}(p-MBA)$_{44}$ and $Au_{\sim 250}$(p-MBA)$_n$, Nanoscale 8 (2016) 18665–18674.
[22] N. Sakaguchi, S. Matsumoto, Y. Kunisada, M. Ueda, Interaction of localized surface plasmons of a silver nanosphere dimer embedded in a uniform medium: scanning transmission electron microscopy electron energy-loss spectroscopy and discrete dipole approximation simulation, J. Phys. Chem. C 123 (2019) 6735–6744.
[23] V. Flauraud, R. Regmi, P.M. Winkler, D.T.L. Alexander, H. Rigneault, N.F. Van Hulst, M.F. García-Parajo, J. Wenger, J. Brugger, In-plane plasmonic antenna arrays with surface nanogaps for giant fluorescence enhancement, Nano Lett. 17 (2017) 1703–1710.
[24] H. Yockell-Lelièvre, F. Lussier, J.F. Masson, Influence of the particle shape and density of self-assembled gold nanoparticle sensors on LSPR and SERS, J. Phys. Chem. C 119 (2015) 28577–28585.
[25] N. Zhang, Y.J. Liu, J. Yang, X. Su, J. Deng, C.C. Chum, M. Hong, J. Teng, High sensitivity molecule detection by plasmonic nanoantennas with selective binding at electromagnetic hotspots, Nanoscale 6 (2014) 1416–1422.
[26] Y. Cheng, M. Wang, G. Borghs, H. Chen, Gold nanoparticle dimers for plasmon sensing, Langmuir 27 (2011) 7884–7891.
[27] D. Liu, L. Fang, F. Zhou, H. Li, T. Zhang, C. Li, W. Cai, Z. Deng, L. Li, Y. Li, Ultrasensitive and stable Au dimer-based colorimetric sensors using the dynamically tunable gap-dependent plasmonic coupling optical properties, Adv. Funct. Mater. 28 (2018) 1707392.
[28] S. Lee, G.H. Gu, J.S. Suh, A simple method to fabricate silver colloid clusters for surface-enhanced Raman scattering, Chem. Phys. Lett. 511 (2011) 121–125.
[29] K. Kim, H. Ryoo, Y.M. Lee, K.S. Shin, Adsorption characteristics of Au nanoparticles onto poly (4-vinylpyridine) surface revealed by QCM, AFM, UV/vis, and Raman scattering spectroscopy, J. Colloid Interface Sci. 342 (2010) 479–484.
[30] H.H. Jeong, N. Erdene, J.H. Park, D.H. Jeong, S.K. Lee, Analysis of fiber-optic localized surface plasmon resonance sensor by controlling formation of gold nanoparticles and its bio-application, J. Nanosci. Nanotechnol. 12 (2012) 7815–7821.
[31] R.P. Bagwe, L.R. Hilliard, W. Tan, Surface modification of silica nanoparticles to reduce aggregation and nonspecific binding, Langmuir 22 (2006) 4357–4362.
[32] D. Mollenhauer, N. Gaston, E. Voloshina, B. Paulus, Interaction of pyridine derivatives with a gold (111) surface as a model for adsorption to large nanoparticles, J. Phys. Chem. C 117 (2013) 4470–4479.
[33] H.M. Kim, J.H. Park, D.H. Jeong, H.Y. Lee, S.K. Lee, Real-time detection of prostate-specific antigens using a highly reliable fiber-optic localized surface plasmon resonance sensor combined with micro fluidic channel, Sens. Actuators B Chem. 273 (2018) 891–898.
[34] L. Xiong, P. Chen, Q. Zhou, Adhesion promotion between PDMS and glass by oxygen plasma pre-treatment, J. Adhes. Sci. Technol. 28 (2014) 1046–1054.
[35] H.M. Kim, S.W. Bae, D.H. Jeong, H.Y. Lee, J.H. Park, S.K. Lee, Comparison of measurement protocol for biosensors using fiber optic localized surface plasmon resonance sensor, Opt. Fiber Technol. 59 (2020) 102324.
[36] J.P. Oliveira, A.R. Prado, W.J. Keijok, P.W.P. Antunes, E.R. Yapuchura, M.C.C. Guimarães, Impact of conjugation strategies for targeting of antibodies in gold nanoparticles for ultrasensitive detection of 17β-estradiol, Sci. Rep. 9 (2019) 1–8.
[37] S.R. Shin, Y.S. Zhang, D.J. Kim, A. Manbohi, H. Avci, A. Silvestri, J. Aleman, N. Hu, T. Kilic, W. Keung, M. Righi, P. Assawes, H.A. Alhadrami, R.A. Li, M.R. Dokmeci, A. Khademhosseini, Aptamer-based microfluidic electrochemical biosensor for monitoring cell-secreted trace cardiac biomarkers, Anal. Chem. 88 (2016) 10019–10027.
[38] S. Celiksoy, W. Ye, K. Wandner, K. Kaefer, C. Sönnichsen, Intensity-Based Single Particle Plasmon Sensing, Nano Lett. 21 (2021) 2053–2058.
[39] K. Takamura, H. Fischer, N.R. Morrow, Physical properties of aqueous glycerol solutions, J. Pet. Sci. Eng. 98 (2012) 50–60.
[40] D. Zhou, K.R. Kittilstved, Electron trapping on Fe^{3+} sites in photodoped ZnO colloidal nanocrystals, Chem. Commun. 52 (2016) 9101–9104.
[41] H.H. Jeong, S.K. Lee, J.H. Park, N. Erdene, D.H. Jeong, Fabrication of fiber-optic localized surface plasmon resonance sensor and its application to detect antibody-antigen reaction of interferon-gamma, Opt. Eng. 50 (2011) 124405.
[42] H. Nguyen Thi Nhat, N.T.T. Le, N.T. Phuong Phong, D.H. Nguyen, M.T. Nguyen-Le, Potential application of gold nanospheres as a surface plasmon resonance

based sensor for in-situ detection of residual fungicides, Sensors 20 (2020) 2229.
[43] Z. Omair, M.A. Talukder, Sensitivity analysis of gold nanorod biosensors for single molecule detection, Plasmonics 14 (2019) 1611–1619.
[44] P.P.A. Suthanthiraraj, A.K. Sen, Localized surface plasmon resonance (LSPR) biosensor based on thermally annealed silver nanostructures with on-chip blood-plasma separation for the detection of dengue non-structural protein NS1 antigen, Biosens. Bioelectron. 132 (2019) 38–46.
[45] C. Mengreli, E. Sarafidou, S. Petmezaki, S. Pantelakis, α-fetoprotein in congenital hypothyroidism, Neonatol. 58 (1990) 326–333.
[46] M. Vercammen, P. Meirlaen, L. Broodtaerts, I.V. Broek, X. Bossuyt, Effect of sample dilution on serum free light chain concentration by immunonephelometric assay, Clin. Chim. Acta 412 (2011) 1798–1804.
[47] J. Kim, S.Y. Oh, S. Shukla, S.B. Hong, N.S. Heo, V.K. Bajpai, H.S. Chun, C.H. Jo, B.G. Choi, Y.S. Huh, Y.K. Han, Heteroassembled gold nanoparticles with sandwich-immunoassay LSPR chip format for rapid and sensitive detection of hepatitis B virus surface antigen (HBsAg), Biosens. Bioelectron. 107 (2018) 118–122.